

Application of Metal–Organic Frameworks for Efficient Removal of Doxorubicin Hydrochloride: Removal Process Optimization and Biological Activity

Kholood M. Alkhamis, Meshari M. Aljohani, Saham F. Ibarhiam, Yasmeen A. S. Hameed, Hana M. Abumelha, Turki M. Habeebullah, and Nashwa M. El-Metwaly*



Cite This: *ACS Omega* 2023, 8, 30374–30388



Read Online

ACCESS |



Metrics & More



Article Recommendations



Supporting Information

ABSTRACT: This study looked at the doxorubicin hydrochloride (DOX) anticancer drug's adsorption characteristics on a silver-based metal–organic framework (Ag-MOF). X-ray diffraction (XRD), scanning electron microscopy (SEM), and X-ray photoelectron spectroscopy (XPS) were used for the characterization of Ag-MOF. The pore volume and surface area of Ag-MOF were determined through Brunauer–Emmett–Teller (BET) testing at 77 K to be 0.509 cm³/g and 676.059 m²/g, respectively. Adsorption at pH 6 was established to be the best for DOX compared to alkaline solution. Ag-MOF has a good capacity for eliminating DOX (1.85 mmol/g), according to adsorption experiments. From the adsorption results, we can find that Langmuir is the most fitted adsorption isotherm model and the pseudo-second order model best fitted the adsorption kinetics. The energy of activation for adsorption, which was determined to be 15.23 kJ/mol, also supported a chemisorption process. The mechanism of adsorption was evaluated, and details of all possible interactions between DOX and Ag-MOF were illustrated. On the other hand, while examining the impact of temperature, we identified the thermodynamic constraints as ΔG° , ΔH° , and ΔS° and confirmed that the reaction was an endothermic one and spontaneous. Even after numerous reuse cycles, the efficiency remained constant. The synthetic adsorbent was remarkably recyclable at a rate of more than 91.6%. By using the MTT assay, the cytotoxicity of the tested Ag-MOF and DOX@Ag-MOF against human breast cancer cells (MCF-7) was evaluated *in vitro*. The *in vitro* antimicrobial activity of Ag-MOF and DOX@Ag-MOF was also tested.



1. INTRODUCTION

Environmental chemistry has recognized the incidence and distribution of pharmaceutically active chemicals in the aquatic environment as one of its developing problems. Pharmaceuticals are constantly entering the situation and are now present at small amounts, which can impair water quality and possibly have an impact on drinking water sources, ecosystems, and human health.¹ The human society and aquatic life are seriously at risk from synthetic chemical pollution of water habitats, which is being caused by expanding manufacturing technology. Many of these kinds of pollutants, sometimes referred to as microcontaminants, show dangerous characteristics even at very low concentrations.^{2,3} Two instances of potentially hazardous compounds that can be discovered in rivers, sediments, lakes, and ground water resources are hospital wastewaters and pharmaceutical factory effluents.⁴ These substances include radionuclides, metabolites, endocrine disruptors, and organic chemicals.

The fact that cytostatic chemotherapeutic medications have the potential to be cancerous, mutagenic, and genotoxic, even at low levels, makes them a particularly problematic class of

pharmaceuticals for the environment.⁵ Doxorubicin hydrochloride (DOX), an antibiotic with an anthracycline ring, is an extremely potent anti-neoplastic drug used in the management of leukemia.⁶ The blatantly hazardous side effects of DOX, including cardiotoxicity, vomiting, baldness, stomatitis, and leucopenia, have made it difficult to use it effectively. In order to reduce side effects without reducing treatment strength, DOX is often encapsulated within drug delivery vehicles that can protect the target molecule and target-specific sections while not adversely affecting the surrounding tissues.⁷

DOX, a potent anticancer agent, is a member of the Adriamycin (ADM) family of medicines, which is frequently used alone or in combination with other medications to treat

Received: May 20, 2023

Accepted: July 27, 2023

Published: August 8, 2023



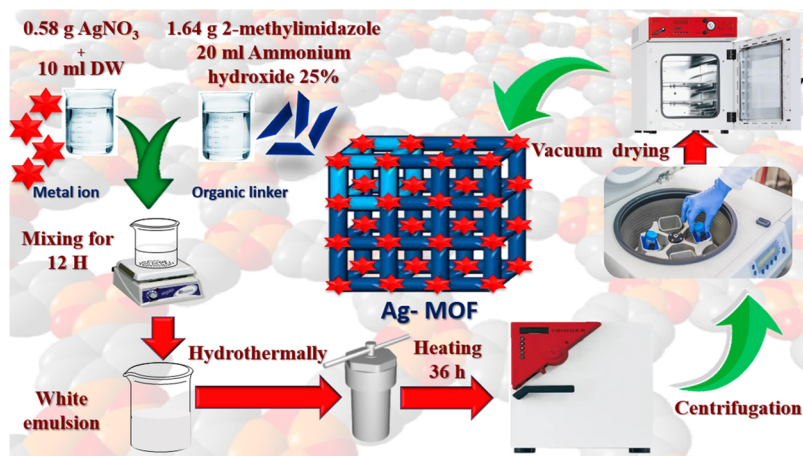


Figure 1. Diagram illustrating the procedures needed to make Ag-MOF.

cancer.⁸ The therapeutic index of DOX is limited by undesirable significant side effects such as myelotoxicity and cumulative cardiotoxicity that occur during the injection of the drug.⁹ In order to minimize the negative effects on healthy organs, the nanoparticle drug delivery system has gained a lot of attention.⁷ A number of nanoparticles have been developed in conjunction with DOX to address this issue and get the best therapeutic results.¹⁰ The removal of pharmaceutical residues in wastewaters has been attempted using a number of treatment techniques, such as membrane techniques, photolytic degradation, improved oxidation, and hybrid techniques.¹¹ Furthermore, secondary contaminants still persist in aqueous solutions as a result of the intricate structures and diverse physicochemical characteristics of DOX.¹² Therefore, a more effective DOX treatment must be developed.¹³

Recently, materials for metal–organic frameworks (MOFs) have received a lot of attention as a result of the wide range of potential uses, which include drug delivery, nonlinear optics, magnetic conductance, gas storage, catalysis, and luminescence.¹⁴ In addition, MOFs are crystalline solids.¹⁵ Furthermore, MOFs based on polyhedral coordination cages are attracting a lot of attention, not just because of their aesthetic appeal but also because the restricted cavities that they provide (i) can be used as a molecular flask to enclose visitor species in a protective shell to prevent chemical reaction, (ii) it is possible to separate and store gases using them, and (iii) it is possible that they will have magnetic and catalytic properties that are uncommon. Based on flexible and porous shape, MOFs' guest ions and molecules, with such metals, can infiltrate into the wholesale material, whereas this guest ions or molecules can be selectively adsorbed due to the shape and size of the pores.¹⁶ Because of their distinct qualities, MOFs are suitable sorbents for removing heavy metals from solid phases by isolating them from other solid phases.¹⁷ In the method of solid phase extraction, however, there is limited knowledge regarding MOFs. Due to the capacity of Ag⁺ ions to permeate cell membranes and interact with thiol containing proteins and DNA, silver was known to be the most excellent antibacterial metal before the development of antibiotics.¹⁸

The increased adsorption capacity and quicker adsorption kinetics of Ag-MOF make it preferable over other MOFs for the elimination of doxorubicin (DOX). The silver ions in Ag-MOF increase the electrostatic contacts between the MOF and the DOX molecules, leading to this the case. Ag-MOF's ability to adsorb materials is further enhanced by the ability of the

silver ions to establish coordination bonds with the functional groups in DOX. Additionally, Ag-MOF has been demonstrated to be stable across a broad pH range, which is critical for real-world applications. Strong metal–ligand interactions between the silver ions and the organic ligands that make up the MOF framework are thought to be the cause of Ag-MOF's stability.

Ag-MOF is also an attractive contender for medicinal applications including drug administration and cancer treatment due to its shown low toxicity and biocompatibility. According to reports, the silver ions in Ag-MOF have antibacterial and antifungal properties that may possibly be useful in biological applications. All things considered, these benefits make Ag-MOF an attractive choice for the removal of DOX and other medicines from wastewater and other environmental matrices. However, as with any treatment approach, the choice of MOF will be based on the particular application requirements and the characteristics of the intended pollutant.¹⁹

In this study, Ag-MOF nanoparticles were created and described in a novel and straightforward manner that produced high-surface-area nanoparticles with a density of 676.059 m²/g and efficiently removed 1043.52 mg/g doxorubicin from wastewater. Even after numerous reuse cycles, this performance remained constant. The adsorbent that was artificially created was remarkably recyclable more than 91.6%. The DOX adsorption on Ag-MOF, which confirmed that the reaction was a chemisorption process and endothermic, was also examined for its kinetic, isothermal, and thermodynamic properties. It was found that the removal efficiency increased as the temperature was increased.

2. RESOURCES AND TECHNIQUES

2.1. Supplies and Characterization. All of the chemicals and equipment's utilized for the elucidation were previously covered in detail (Supporting Information).¹⁹

2.2. Ag-MOF Nanoparticle Synthesis. Complementary silver-based metal–organic frameworks were created by dissolving 1.64 g of 2-methylimidazole in 20.0 mL of ammonium hydroxide 25% and 0.58 g of AgNO₃ in 5 mL of distilled water. The two separate solutions were mixed for 12 h, followed by a conventional hydrothermal synthesis procedure following full dissolution.²⁰ The resulting mixture was heated for 36 h at 100 °C (5 °C/min heating rate) in a Teflon autoclave with a 100 mL wall. The material was centrifuged

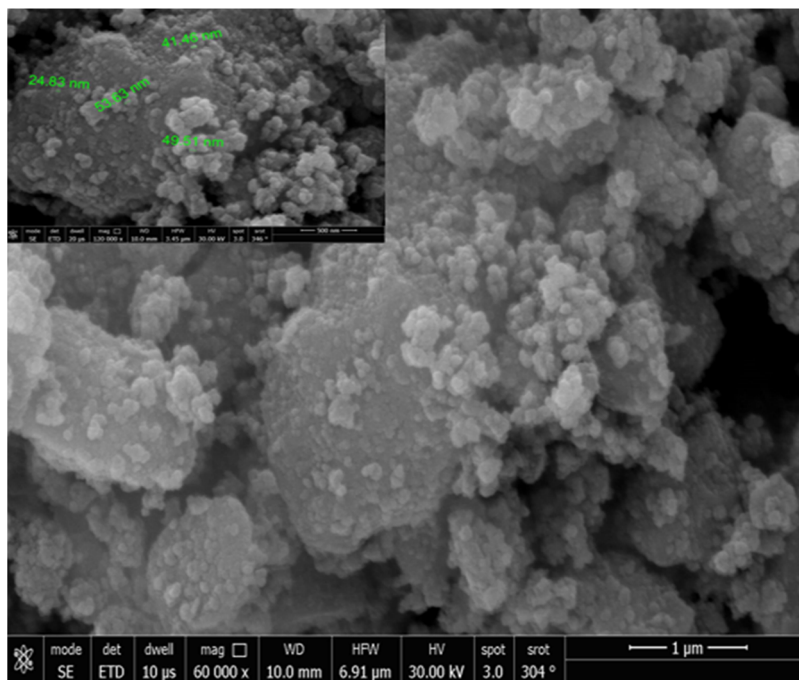


Figure 2. Nanoparticles of Ag-MOF captured via SEM.

after cooling, thoroughly cleaned twice with deionized water, and then vacuum-dried at 80 °C overnight (Figure 1).

2.3. Studies on Batch Adsorption Experiment Design.

The Ag-MOF samples were dispersed in all batch adsorption trials (adsorbent amount = 0.02, 0.05, 0.10, 0.15, and 0.20 g) in 25 mL of DOX solution (concentration = 2.76×10^{-4} to 2.2×10^{-3} mmol/L), allowing them to react at a range of temperatures (293 to 323 K) and pH values (3 to 10). All of the investigations have been carried out in a thermostatic shaker for the water bath with the reaction vessel spinning at 100 rpm.²¹ The adsorbed Ag-MOF samples were acquired using a centrifuge after a predetermined adsorption time, the supernatant was filtered, and the DOX level was measured at 380 nm by UV–vis spectroscopy. The equilibrium period of adsorption for DOX on Ag-MOF was determined by these tests to be 100 min. To avoid DOX from photodegrading throughout the batch tests, sample flasks and tubes were covered through aluminum foil.^{22,23} To determine the extraction yield and amount of DOX adsorbed on Ag-MOF, eqs 1 and 2 were used (Table S1) (Supporting Information).

$$R\% = \frac{(C_0 - C_t)}{C_0} \times 100 \quad (1)$$

$$q_e = \frac{(C_0 - C_e)V}{M} \quad (2)$$

3. RESULTS AND DISCUSSION

3.1. Description of Ag-MOF. **3.1.1. X-ray Diffraction (XRD) Patterns.** A quick analytical method for determining the crystal structure, phase purity, and chemical make-up of an unidentified material is X-ray diffraction (XRD). The Ag-MOF material's as-prepared XRD pattern is shown in Figure S1 (Supporting Information).^{24,25} The synthesized Ag-MOF's solidity was examined using XRD, which shows the XRD patterns of Ag-MOF acquired at a scan range of 5–70° (Figure

S1). The XRD pattern of Ag-MOF displayed strong and sharp peaks at 2θ values of 16.22, 16.78, 20.02, 27.89, 28.55, 29.778, and 23.80°, indicating a high degree of crystallinity. According to simulations made with the help of the Foolproof and Check Cell software, the Ag-MOF's crystal systems has a monoclinic crystal structure within the space group $P2_1/C$. The following calculations were also used for determining the degree of crystallinity: $a = 12.22 \text{ \AA}$, $b = 6.28 \text{ \AA}$, $c = 10.91 \text{ \AA}$, $\alpha = 90^\circ$, $\beta = 114.45^\circ$, and $\gamma = 90^\circ$. Table S2 gifts the Miller indices (hkl) and interplanar spacing (d_{hkl}) of Ag-MOF. Our findings further show that the Ag-MOF nanospheres' diffraction peaks were preserved after adsorption, suggesting that their crystal structure is quite strong (Table S2).

The XRD measurements demonstrate that the Ag-MOF has a substantially crystalline form (Figure S1) (Supporting Information). This is corroborated by the formation of a noticeable peak at 28.16°, which is characteristic of coordination compounds with an Ag-organic component. Minor peaks were also visible at 10.9, 11.8, 13.04, 17.1, and 33.97°. The peaks of the face-centered cubic crystal planes of Ag-MOF nanoparticles appeared at 39.16, 43.84, and 65.31° within the (111), (200), and (220) peaks, respectively (Table S2).²⁶

3.1.2. Brunauer–Emmett–Teller (BET). N_2 adsorption–desorption isotherms were created to measure the pore volume and the surface area of the Ag-MOF pore before and after DOX adsorption (Figure S2a) (Supporting Information). Our results support the synthesis of a Ag-MOF adsorbent having microporous holes and the formation of DOX@Ag-MOF upon DOX adsorption. The type II feature of adsorption/desorption isotherms exhibits sharpness and aids in the creation of microporous materials. Hysteresis loops are classified as type H3 loops. As indicated in Figure S2b, the pore size of Ag-MOF was decreased after adsorption of DOX from 1.609 to 1.572 nm. Our results after adsorption presented that the surface area of Ag-MOF meaningfully decreased. The surface area of the Ag-MOF was estimated to be (482.650

m^2/g following DOX adsorption, which is smaller than the $676.059 \text{ m}^2/\text{g}$ of pure Ag-MOF.²⁴

3.1.3. SEM Examination. A scanning electron microscopy (SEM) picture was used to inspect the crystal particle sizes and shapes as a result of the reaction circumstances. The distribution and adsorption of DOX depends greatly on the surface area and shape. The SEM analysis proved that Ag-MOF on average represented a nanoparticle with its diameter extending from 24.83 to 53.63 nm (Figure 2). This result demonstrated how clusters of small nanoparticles might develop. Considering the number of Ag-MOF pores, it is likely that DOX adsorption will get trapped there.^{19,27}

3.1.4. XPS. The δ -phase of Ag-MOF is more thoroughly studied with the aid of a supplementary method like X-ray photoelectron spectroscopy (XPS). Considering the oxidation states and chemical relationships between the elements, this can provide crucial information. Figure S3 (Supporting Information) displays the Ag 3d, C 1s, N 1s, and O 1s states of the pure Ag-MOF at various core energy levels. Two peaks in the Ag 3d spectrum that correspond to the Ag $3d_{5/2}$ and Ag $3d_{3/2}$ core energy levels have been seen (spin-orbit coupling), whose binding energies are 368.47 and 374.4 eV, respectively (Figure S3).

Two peaks at 531.2 and 532.4 eV energy sites in the O 1s spectrum (Figure S3) represent oxygen in the $\text{O}=\text{C}-\text{OH}$ and $\text{C}-\text{O}$ phases, respectively.²⁸ Our primary conclusion from the XPS data is that the core energy stages of Ag-MOF (Figure S3) appeared at a slightly higher affinity energy than those stated in the literature.²⁹ This disparity results from the difficulties in comprehending X-ray emission from metals because the d energy bands are situated a few electron volts slightly below the Fermi energy level. The core energy peaks indicated a shift to the more energetic side after combining Ag-MOF (Figure S3). This demonstrates that the electron density at an atomic site is lower than that of simple ionic substances. It is observed that the Ag-d-band of MOF photoemission spectra is narrower than that of regular Ag (Table S3) (Supporting Information).²⁹

The accumulation of positive charges left behind via photoelectrons produced by the sample surface shifts the binding energy of photoemitted electrons. To charge-correct a spectrum, one employs the reference binding energies of carbon and, more typically, silver. The typical uncharged BE of C 1s is 284.8 and is used as a reference because C exists as adsorbed carbon on each XPS specimen that we evaluate. It implies that the BE along axis has to be charge-corrected using the C 1s peak at 284.8 eV and then adjusted. The corrected peaks of all other peaks in the same spectrum are identical. Applying the C 1s shift to other peaks is all that is necessary, like the one in our example, in an alternate spectrum, $284.8 - 284.47 = 0.33 \text{ eV}$. It should be moved by 0.33 eV to account for all peaks.³⁰

3.1.5. Point of Zero Charge. The point of zero charge (PZC) in the elimination of DOX was used to assess the charge on the Ag-MOF surface. According to our studies, the pH_{PZC} for the Ag-MOF was 4.9.³¹ The pH_{PZC} is shown in Figure 3 with the initial pH on the X-axis and the $\text{pH}_{\text{final}} - \text{pH}_{\text{initial}}$ difference on the Y-axis.

3.2. Experiments with the Batch Process. **3.2.1. Impact of pH.** In general, the process is examined through the pH of an aqueous solution, and it can have a direct impact on the adsorbent's ability for DOX with concentration $1.7 \times 10^{-3} \text{ mol/L}$. The adsorption of DOX in water by Ag-MOF at various pH levels is presented in Figure S4 (Supporting

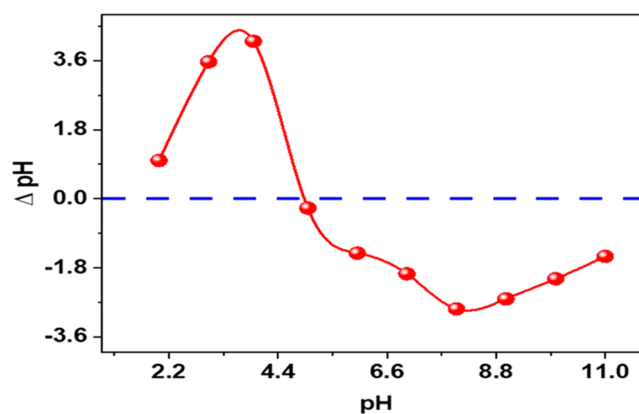


Figure 3. Ag-MOF point of zero charge (pH_{PZC}).

Information). Therefore, pH directly influenced the Ag-MOF DOX's adsorption ability. The best clearance of DOX was 1.38 mmol/g at pH 6. Since the zero-charge point (pH_{PZC}) occurred at pH 4.9, Ag-MOF is negatively charged at $\text{pH} > 4.9$ and therefore electrostatic interactions helped to favorably adsorb positively charged DOX, resulting in the greater elimination efficiency at pH 6 that was found. This increased the adsorption effectiveness by increasing the amount of interaction between both the negatively charged Ag-MOF and the positively charged DOX ions. This data revealed that electrostatic interactions in these pH ranges are incapable of explaining the adsorption mechanism.³²

3.2.2. Influence of Adsorbent Dose. The results of the investigation into the dose effects of Ag-MOF on DOX adsorption are shown in Figure 4. DOX adsorption is

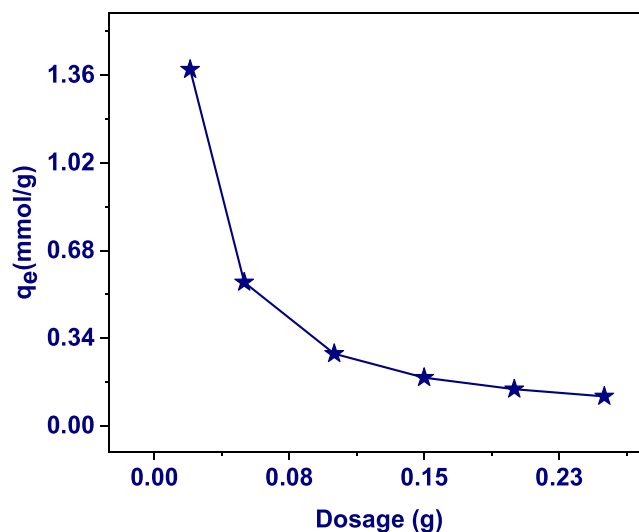


Figure 4. Amount of Ag-MOF utilized affects the adsorption of DOX: absorption capacity vs SD (conc. $1.77 \times 10^{-3} \text{ mmol/L}$, temp. $25 \text{ }^\circ\text{C}$, dose 0.02 to 0.25 g, volume 25 mL, pH 6, and time 45 min).

influenced by the amount of Ag-MOF utilized: (i) adsorbent capacity vs standard deviation and (ii) adsorbent dose vs comparative remaining concentration (C/C_0). The q_e of Ag-MOF rapidly reduced from 1.38 to 0.11 mmol/L, while the amount of Ag-MOF was raised from 0.02 to 0.25 g. Increasing Ag-MOF dosages resulted in more readily available reactive groups, which boosted DOX's ability to adsorb in an aqueous solution. However, too much adsorbent effectively restricted

the usage of adsorption sites, making them undesirable. This led toward the conclusion that the ideal dosage for the adsorption experiments was 0.02 g of Ag-MOF.³³

3.2.3. Impact of DOX Concentration. The original DOX concentration also affects how well the removal works using different DOX doses at pH 6. Along with an increase in DOX quantity, the drug adsorption sites grew. As the concentration rises, more molecules come into contact with the Ag-MOF surface, increasing the amount of DOX that can be adsorbed. The fact that there were a large number of potential adsorption sites on the adsorbent that were sufficient to totally successfully absorb DOX at the lower initial DOX concentration resulted in notable removal rates.³⁴ However, DOX concentrations increased, less adsorption sites were relatively accessible on the substance's surface, and those that were still there were not enough to successfully bind DOX. A lot of these locations were rapidly filled.

3.2.4. Contact Time Effect. The effect of the contact time, which extended from 5 to 100 min, on DOX adsorption was studied (Figure S5) (Supporting Information). According to our findings, DOX removal increased over time and saturated at 100 min. According to our results, the DOX sorption degree is fairly high inside the first hour of adsorption, which might be owing to Ag-MOF's large surface area and availability of active centers. This efficient adsorption is also caused by these properties. The pores of Ag-MOF and active sites were depleted, which caused the DOX sorption rate to stabilize (Figure 5).³⁵

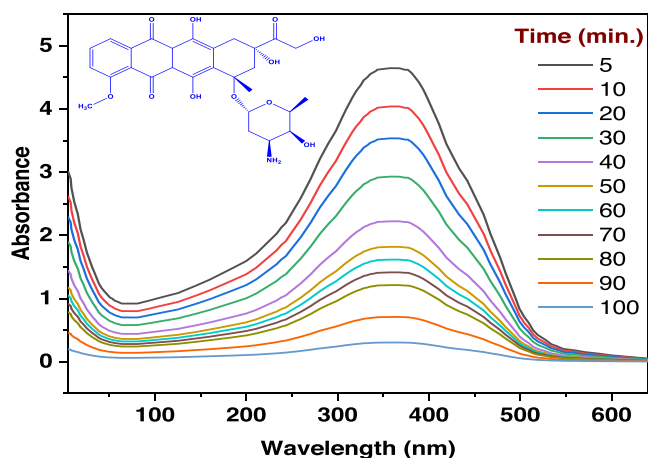


Figure 5. UV spectrum of DOX adsorption at different time intervals (conc. 1.9×10^{-3} mmol/L, dose 0.02 g, volume 25 mL, temp. 25 °C, pH 6, and time 45 min).

3.2.5. Temperature Effect. When the temperature rises from 20 to 45 °C, more DOX is adsorbing against Ag-MOF (q_e , mmol/g) (Figure S6) (Supporting Information). Our results imply that the elimination process is endothermic because the amount of DOX adsorbed onto Ag-MOF rises with rising temperature. As the temperature increases, there was an increase in DOX diffusion over surface sites and inside Ag-MOF pores.

3.2.6. Adsorption Isotherms. It is an essential technique for analyzing how such an adsorbate disperses from the liquid to the stationary surface up to equilibrium under predetermined (measured) parameters. Diverse adsorption isotherms have been used to explore the isotherm kind, the adsorption process, the adsorbent sensitivity, the type of interaction

(monolayer or multilayer), and the optimal adsorption ability. Six models, namely, Langmuir,³⁶ Freundlich,³⁷ Dubinin–Radushkevich (D–R),³⁸ Redlich–Peterson,³⁹ Harkin–Jura, and Temkin, were used.⁴⁰ Several methods were used to fit the experimental results (Table 1). The Langmuir model is predicted based on three factors: single-layer adsorption, equivalent adsorption sites, and the adsorption of each molecule on the adsorbent active sites occur regardless of the total occupancy of that molecule. Defiantly, under the Freundlich model, an experimental equation proposed that the active places of the adsorbent are heterogeneous and that multilayer construction is likely. The Temkin model implies a linear fall in adsorption energy, which is the opposite of what the Freundlich isotherm model predicts (Figure 6). The Dubinin–Radushkevich model may be able to determine this sort of adsorption procedures because of the form of the porous Ag-MOF and the quantity of energy required. The result of this isotherm reveals that, the means values of sorption's energy is 15.25 kJ/mol. The characteristics of the Langmuir and Freundlich isotherms are combined in the Redlich–Peterson (R–P) model. Redlich–Peterson recommended a three-parameter adsorption isotherm calculation where K (L/g), a , and n characterize the Redlich–Peterson coefficients and n displays a factor that is between 0 and 1. The Langmuir isotherm, which enjoys infinite dilution and approaches the Henry zone, acts as the numerator's foundation. This empirical isotherm model has three variables. By mixing components of the Langmuir and Freundlich formulas, it produces a varied adsorption process that varies because of perfect monolayer adsorption. This isotherm model suggests adsorption equilibrium more than a broad range of DOX concentrations because it is adaptable and has a linear relation on concentration in the fraction and an exponential meaning in the quantity. It works well in both consistent and varied environments. A different hypothesis is that multilayer adsorption occurs on the surface of absorbents consuming heterogeneous pore delivery according to the Harkin–Jura isotherm equation.

In every instance, the fitting coefficients mirrored the following pattern: $R_L^2 > R_R^2 > R_F^2 > R_T^2 > R_D^2 > R_H^2$. It was determined that the Langmuir model was best suitable. A single layer was where the majority of the adsorption took place. The separation influence, R_L (dimensionless), may have been used to assess whether an adsorption mechanism was fitting for a Langmuir isotherm model. A value of $R_L = 0$ is evidence that the adsorption was permanent, $0 < R_L < 1$ demonstrates that it was an excellent candidate for adsorption, $R_L = 1$ means that a straight line was followed during the adsorption, and $R_L > 1$ signifies that there was no way for adsorption to occur in the arrangement. As shown in Table 1, the R_L standards (0.006–0.050) were all inside the range of 0–1, demonstrating that the adsorption procedure was effective. In the Freundlich model, n is a variable that changes with temperature, and the anisotropic influence is $1/n$. A value of $0 < 1/n < 1$ preferred the DOX elimination, $1/n = 1$ demonstrates that there remained no interaction among the adsorbate and adsorbate during the adsorption process, and $1/n > 1$ implies a difficult adsorption process. Table 1 shows the results; the values of $0 < 1/n < 1$ confirmed that the adsorption occurred without effort, and this matched the Langmuir model's findings. Temkin's isotherm makes use of the connections between the adsorbate and the adsorbent and accepts a linear decrease in adsorption heat. The Temkin

Table 1. Isothermal Conditions for DOX Adsorption over Ag-MOF at 25, 35, and 45 °C

models		25		35		45	
		linear	nonlinear	linear	nonlinear	linear	nonlinear
Langmuir	$q_{m \text{ exp}}$ (mmol g ⁻¹)	1.316		1.564		1.85	
	q_m (mmol g ⁻¹)	1.338	1.37	1.59	1.62	1.88	1.841
	K_L (L mmol ⁻¹)	237,898.1	127,895.34	236,973.58	247,862.71	64,084.33	74,633.46
	R_L	(0.015–0.002)		(0.015–0.0023)		(0.05–0.007)	
	R^2	0.9994	0.97	0.9995	0.92	0.9991	0.987
Freundlich	n	5.07	2.23	3.95	2.12	3.73	6.17
	K_F (mmol g ⁻¹)(L mmol ⁻¹) ^{1/n}	6.83	6.48	13.56	12.86	15.79	8.9
	R^2	0.686	0.731	0.773	0.68	0.774	0.856
Dubinin–Radushkevich	Q_{DR}	1.047	0.962	1.45	1.12	1.55	2.6
	K_{DR} (J ² mol ⁻²)	-1.76×10^{-9}	-1.86×10^{-9}	-2.349×10^{-9}	-2.26×10^{-9}	-2.349×10^{-9}	-2.29×10^{-9}
	E_a (kJ mol ⁻¹)	15.25	14.62	14.84	14.12	14.58	13.8
	R^2	0.982	0.991	0.8435	0.822	0.863	0.82
Temkin	b_T (L mol ⁻¹)	14,660.2	18,782.05	10,237.6	11,328.7	8736.51	8842.71
	A_T (kJ mol ⁻¹)	16.15	11.62	14.822	13.99	14.31	13.68
	R^2	0.778	0.997	0.84	0.881	0.923	0.954
Harkin–Jurra	A	59.5	68.33	0.1623	2.4	0.588	0.62
	B	-322.62	-292.6	-0.29	-0.18	-3.5	-3.2
	R_H^2	0.333	0.509	0.37	0.74	0.41	0.74
Redlich–Peterson	β	0.77	0.69	0.7958	0.72	0.8426	0.822
	A	11.47	10.88	8.58	7.86	4.9	4.3
	R_R^2	0.949	0.886	0.949	0.82	0.955	0.96

constant b_T was 9067 L/mol and A_T was 14.089 kJ/mol, and it is confirmed that the adsorption mechanism is physiochemical in character. Depending on the R^2 values, Temkin's isotherm did not fit the data that was gathered and reviewed. The application of Langmuir and Freundlich is advantageous for both homogeneous and heterogeneous mechanisms, and a distinct model (Redlich–Peterson isotherm) is a better version of this concept. As a result, Table 1 shows that the Freundlich isotherm model is confirmed if the value of the exponent β_R tends to 0, while the Langmuir isotherm is followed if the exponent value of β_R is within 1. The calculated value of β_R designed for the adsorption of DOX on Ag-MOF also serves as confirmation that the adsorption favors the Langmuir isotherm model.^{25,41}

Finally, while these models can be useful in describing adsorption processes, it is significant to be aware of their limits and to use them appropriately. It is also important to consider other factors that may affect adsorption, such as the surface chemistry of the adsorbent, the morphology of the adsorbent, and the nature of the adsorbate. Additionally, it may be necessary to use more complex models or combinations of models to accurately represent adsorption under certain conditions. Ultimately, the choice of model should be based on a careful consideration of the specific experimental conditions and the goals of the study. And on other hand, the adsorption isotherm was fitted to Langmuir at linear and nonlinear forms (Figure 7).

3.2.7. Adsorption Kinetics. Intended for a complete considerate of the sorption procedure from the perspective of design, adsorption kinetics studies are necessary. These studies define the adsorption reaction pathway, equilibrium (saturation) time, and all of the processes in the liquid–solid interface that can regulate the DOX and Ag-MOF interaction. They help researchers by laying the foundation for creating commercial adsorption systems. The resulting data was examined using four commonly used kinetics models in instruction to construct the most suitable kinetics model encompassing the kinetics adsorption characteristics: the

pseudo-first-order rate equation (PFORE),⁴² pseudo-second-order rate equation (PSORE),⁴³ intraparticle diffusion (IPDE),⁴⁴ and Elovich models.⁴⁵

Table 2 shows the DOX adsorption kinetics for Ag-MOF along with model constants and correlation coefficients. According to Figure 8, the PSORE kinetic model was found to be the most successful of the kinetic models investigated. The model with the greatest degree of correlation ($R_{2nd}^2 > R_{1st}^2$) and the best fit to the experiment's information. Furthermore, these results demonstrated that DOX adsorption at Ag-MOF was mostly carried out through chemical adsorption between Ag-MOF and DOX molecules employing valence forces, such as electron sharing or exchange. The intraparticle diffusion model was used to fit all of the data and characterize the diffusion of DOX inside Ag-MOF. As shown in Figure 8, the DOX adsorption by Ag-MOF might be evidently divided into three linear zones with different slopes. The fact that the appropriate lines did not cross at zero further suggests that the adsorption mechanism involves many steps.^{46–48} Throughout the first phase, boundary layer diffusion quickly transferred the DOX to the Ag surface of MOFs.²³ However, the DOX molecules kept moving into the Ag-MOF holes that were being exploited as adsorptive sites during the second step. During the final phase, adsorption equilibrium was reached (Figure 9).

The PFORE, PSORE, IPD, and Elovich models were used to evaluate the interaction time impact and its order in the setting of adsorption kinetics in an attempt to accurately portray the DOX speed of diffusion and their governing stage, considering that the rate of the adsorption process is directly proportionally influenced by the difference between q_e and q_t . In the meantime, PSORE proposed that the adsorption procedure is governed by a chemisorption mechanism including the exchange or transfer of electrons among the adsorbent surface and adsorbate. The linearized fitting was used to fit the data as shown in Figure 8, and nonlinear reversion was utilized to carefully assess the model's suitability (Figure 9). It is straightforward to conclude that the results of

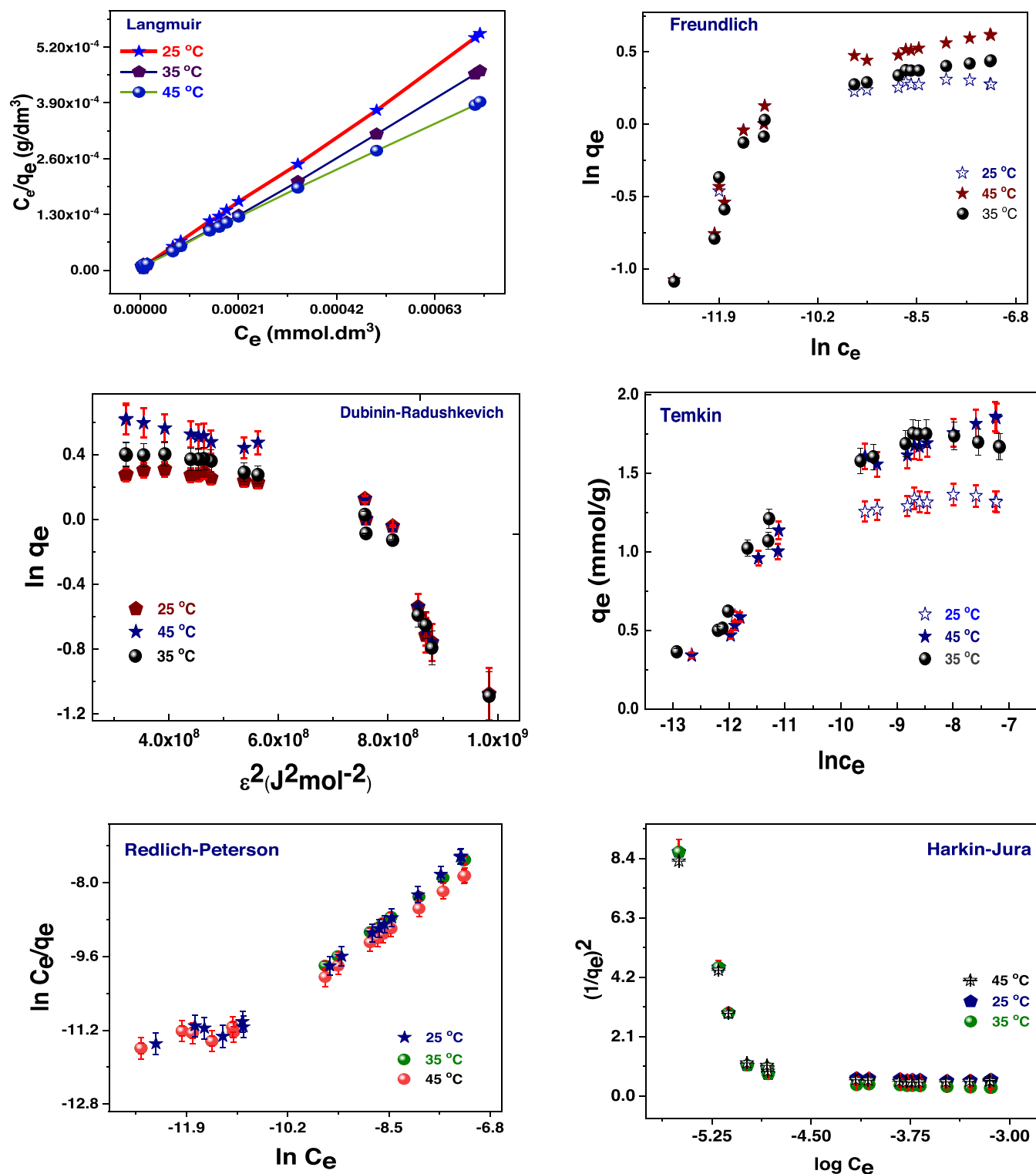


Figure 6. Models for the linear form of the adsorption isotherm of DOX onto Ag-MOF. (Conc. 2.76×10^{-4} to 2.2×10^{-3} mmol/L, dose 0.02 g, volume 25 mL, temp. 25 °C, pH 6, and time 45 min).

DOX adsorption onto Ag-MOF were fitted with PSORE and are more reliable to be corresponding with the PSORE model by associating the considered (R^2) values given in Table 2 for both cited models.^{49,50}

Theoretically, the adsorbate needs to pass through three major stages in order to migrate the bulk solution into the adsorbent (solid) surface (Figure 10): (i) Film dispersion is the external transport of DOX molecules across the bulk

solution toward the Ag-MOF surface. (ii) Ag-MOF pores allow DOX molecules to diffuse across and occupy the adsorptive locations (intraparticle dispersion). (iii) Once DOX molecules are evenly dispersed on the surface of the positively charged Ag-MOF, they bond to it strongly. Utilizing the IPD model, the rate-limiting phases in the DOX adsorption method were investigated. The mass is transferred through the exterior liquid film of the adsorbent, and then adsorbate molecules are

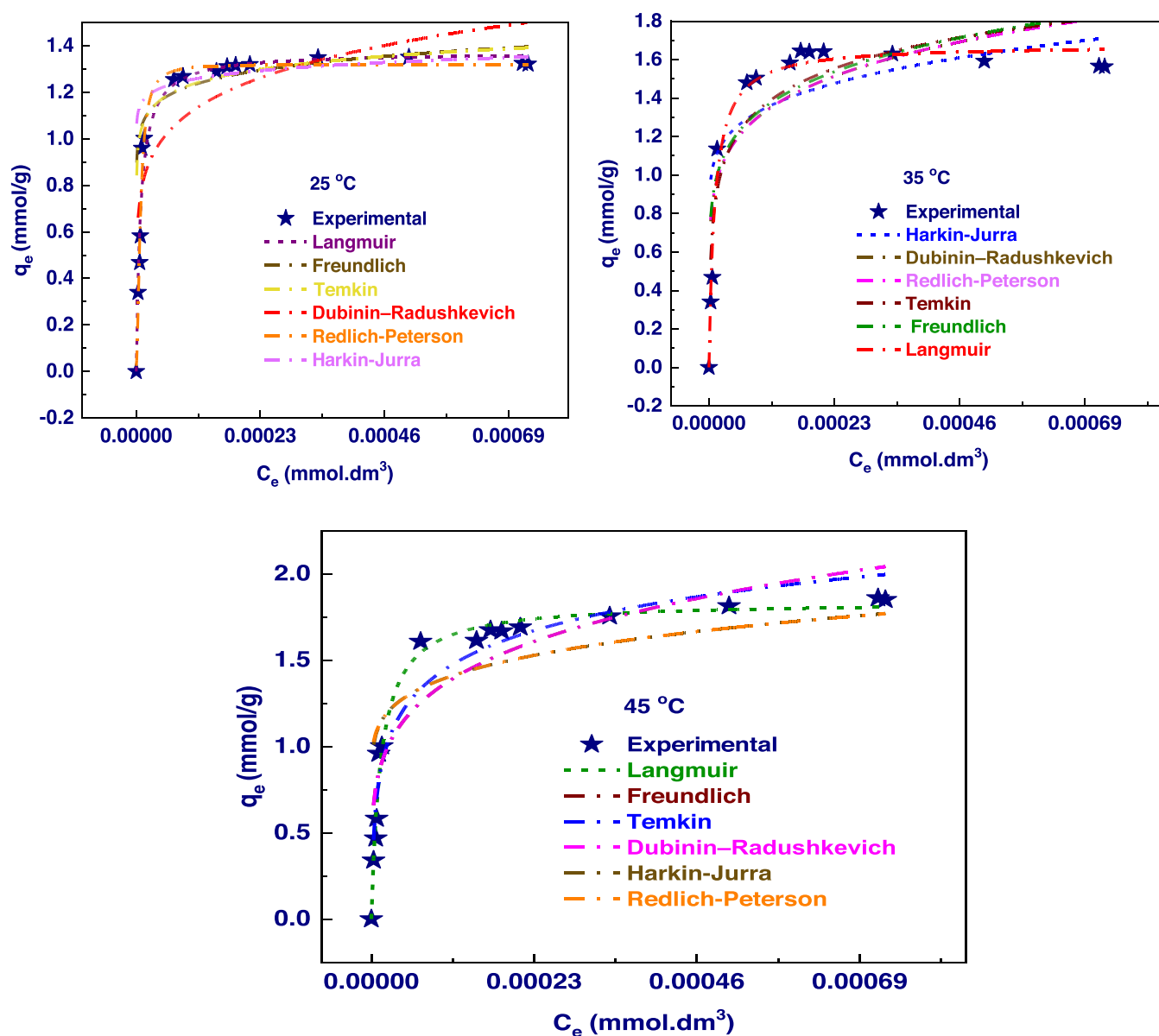


Figure 7. Models for the nonlinear form of the adsorption isotherm of DOX onto Ag-MOF. (Conc. 2.76×10^{-4} to 2.2×10^{-3} mmol/L, dose 0.02 g, volume 25 mL, temp. 25 °C, pH 6, and time 45 min).

Table 2. Adsorption of DOX onto Ag-MOF Adsorbent Kinetic Parameters at 25, 35, and 45 °C

temp		25 °C		35 °C		45 °C	
expt data	q_e (exp) (mmol g ⁻¹)	1.35		1.57		1.848	
model	parameters	linear	nonlinear	linear	nonlinear	linear	nonlinear
pseudo-first-order kinetic	K_1 (min ⁻¹)	0.0144	0.011	0.0152	0.11	0.528	0.68
	q_e (mmol g ⁻¹)	0.536	0.47	0.18	0.17	0.528	0.638
	R^2	0.898	0.973	0.892	0.92	0.899	0.923
pseudo-second-order kinetic	K_2 (g mg ⁻¹ min ⁻¹)	0.97	0.904	0.36	0.902	0.16	0.12
	q_e (mmol g ⁻¹)	1.313	1.315	1.49	1.505	1.8	1.793
	R^2	0.999	0.987	0.999	0.956	0.999	0.834
intraparticle diffusion	K_i (mg g ⁻¹ min ^{1/2})	0.00228	0.07	0.053	0.058	0.09	0.092
	X (mg g ⁻¹)	1.12	0.732	1.04	0.996	0.935	0.911
	R^2	0.995	0.462	0.996	0.862	0.995	0.557
Elovich	β (g/mg)	4.16	4.12	7	7.8	16.7	15.12
	α (mg g ⁻¹ min ⁻¹)	1.89	1.82	2.39	2.08	2.82	3.9
	R^2	0.926	0.982	0.927	0.931	0.928	0.98

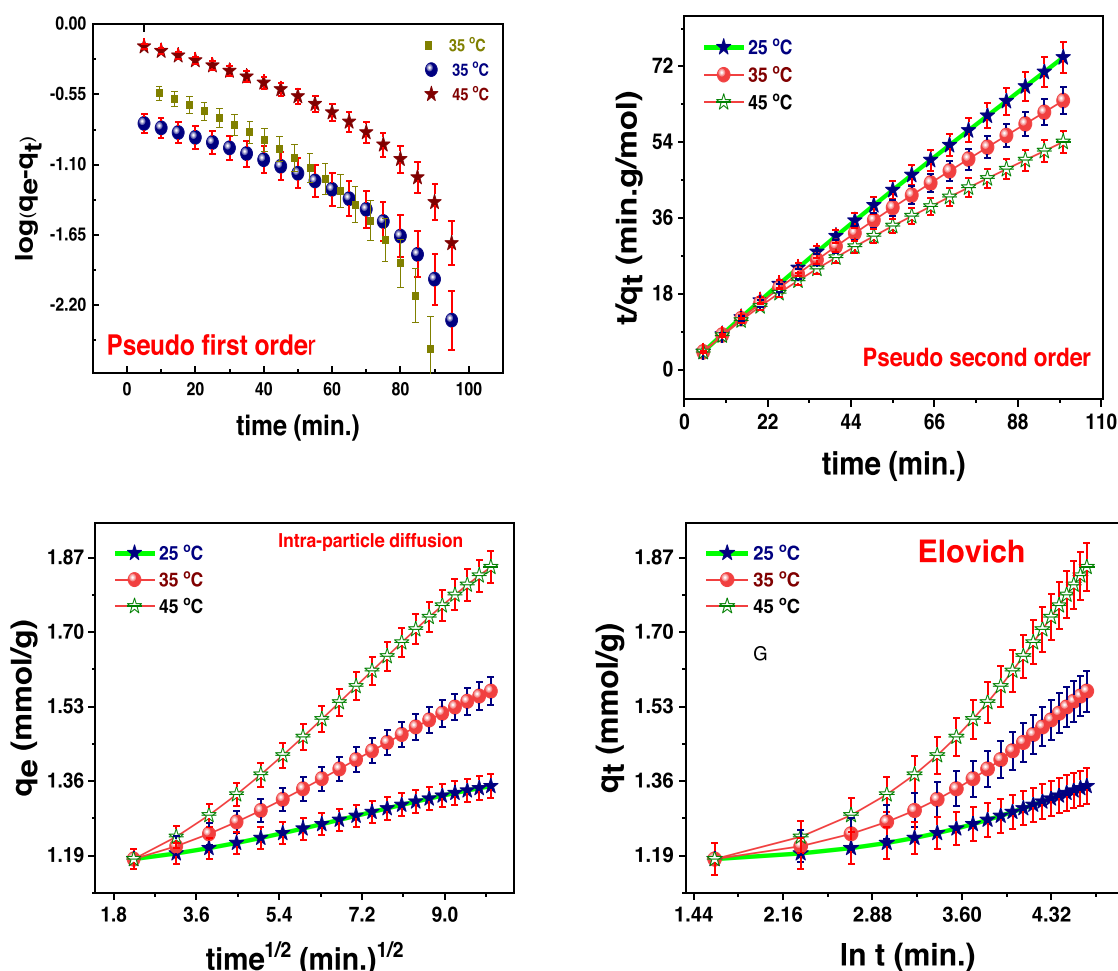


Figure 8. Adsorption kinetics of DOX onto Ag-MOF (linear form). (Conc. 1.9×10^{-3} mmol/L, dose 0.02 g, volume 25 mL, temp. 25 °C, pH 6, and time 45 min).

transported inside the particles. Many phases in the adsorption procedure on a porous adsorbent culminate in adsorption upon the internal or exterior sites of the adsorbent via physical or chemical bonding. Assuming that the final step is a rapid procedure, film or intraparticle diffusion is projected to have the biggest impact upon the adsorption rate. In order to understand the mechanism adsorption procedure, the IPD was adjusted by graphing q_t vs $t^{0.5}$. The adsorption regulatory mechanism is IPD only if the mathematics equal to zero (*i.e.*, passes through the origin) on depicted line. On the other hand, additional processes, such as liquid film diffusion, could be utilized to control the adsorption procedure if it fails to diffuse through the source. The Elovich equation was developed to demonstrate how the heterogeneity of the adsorptive sites affects the variance in adsorption energies across them.²⁶

3.2.8. Adsorption Thermodynamics. For the practical usage of adsorbents, it is imperative to comprehend how temperature affects adsorption. The adsorption testing was done at temperatures between 20 and 45 °C (Figure S7) (Supporting Information). The capability of Ag-MOF to absorb DOX became more effective from 0.6 to 0.8 mmol/L as the temperature increased from 20 to 45 °C, as a result.^{3,51} Through considering the thermodynamic values of parameters, comprehensive and insightful observations on the thermodynamic properties, particularly spontaneity, are made. It is easy to research the viability and reaction type, whether exothermic

or endothermic.⁴⁹ Change in free energy of adsorption (ΔG°) is calculated using the following equation

$$\Delta G^\circ = \Delta H^\circ - T\Delta S^\circ \quad (3)$$

Consequently, the van't Hoff equation is eq 4

$$\ln K_{eq} = \frac{-\Delta H^\circ}{RT} + \frac{\Delta S^\circ}{R} \quad (4)$$

Our results could be clarified by the detail that when the temperature rises, the mobility and rate of diffusion of DOX molecules through the surface of the adsorbent increase. Table 3 displays the conclusions of the analyses of the key thermodynamic parameters. The endothermic nature of the adsorption mechanism is confirmed by the positive value of ΔH° , and the negative value of ΔG° suggests a spontaneous adsorption response. The growth in the negative value of ΔG° as the temperature rises approves that the viability of the reaction increases with temperature, and the fact that ΔS° is positive shows that the system gets more randomness following DOX adsorption. The range of the adsorption temperature can be expected using the temperature where the standard free energy is zero (T_0). The lowest temperature needed for the mechanism to spontaneously operate might be found. The designed value of T_0 was 286.68 K. The low T_0 value shows that the examined adsorbents are capable of DOX adsorption at very low temperatures (eq 5).

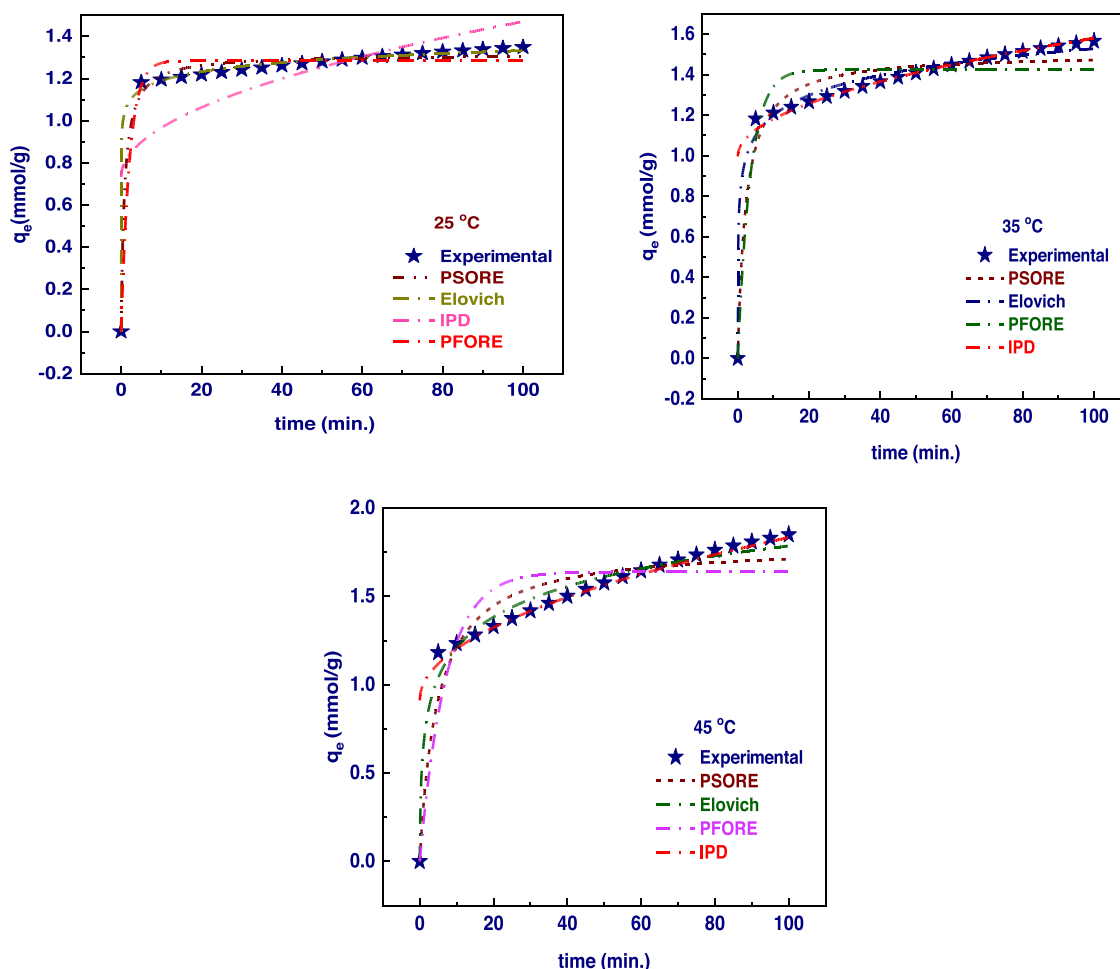


Figure 9. Adsorption kinetics of DOX onto Ag-MOF (nonlinear form). (Conc. 1.9×10^{-3} mmol/L, dose 0.02 g, volume 25 mL, temp. 25 °C, pH 6, and time 45 min).

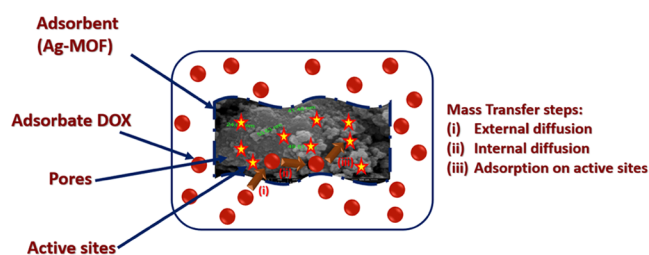


Figure 10. Diagrammatic representation of the dispersion of DOX on Ag-MOF.

$$K_c = \frac{q_e}{C_e} \quad (5)$$

3.2.9. Interaction Mechanism. The method of adsorption in the present study is normally anticipated based on the results of the evaluation of the kinetic and isotherm studies. According to the best fits of the pseudo-second kinetics and Langmuir isotherm models, it has been demonstrated that

DOX absorption and removal by the adsorbent entail a significant chemisorption sorption process. A much more electronegative N atom may result in a reduction in the amount of π electrons present on the adsorbent's surface, enhancing Ag-MOF's ability to receive electrons and making DOX elimination easier. To enhance adsorption, DOX interacts with Ag-MOF as a π - π electron donor-acceptor. Due to its enrichment of electrons, DOX is frequently regarded as a π donor. Furthermore, the greater surface area and pore volumes of Ag-MOF greatly aid in the adsorption of DOX via a pore-filling procedure (Figure 11).⁵²⁻⁵⁴

3.2.10. Ag-MOF Recycling for DOX Elimination. Every substance with porosity, including MOFs, ought to be reusable for practical use. An adsorbent is considered cost-effective if it can be used repeatedly while maintaining its ability to remove, separate, and recover DOX after regeneration. Adjusting the pH is the most typical technique for desorbing DOX. Ag-MOF was carefully rinsed with 0.1 M HCl or 0.1 M NaOH several times until the pH of the detergent mixture reached 7 in order to refresh the sample sorbent. The adsorbent was then

Table 3. DOX Adsorption on the Ag-MOF Adsorbent is Subject to Thermodynamic Restrictions

ΔH° (kJ/mol)	ΔS° (J/mol-K)	T_0 (K)	$-\Delta G^\circ$ (kJ/mol)				
			293 K	298 K	303 K	308 K	318 K
19.89	74.04	286.68	1.80	2.17	2.54	2.90	3.65

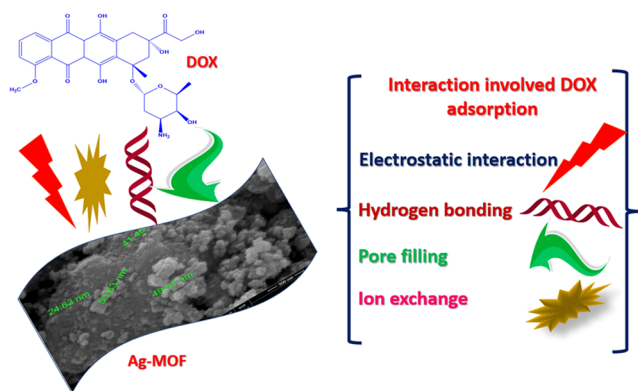


Figure 11. How Ag-MOF eliminates DOX from an aqueous solution through adsorption.

repeatedly cleaned with distilled water and methanol.^{55,56} After being roasted for 4 h at 60° C, the clean Ag-MOF was obtained. The adsorbent was employed in the subsequent DOX adsorption experiment after becoming regenerated. The adsorbent's regeneration effectiveness was found to be 98.2% for every adsorption/desorption cycle (Table 4). A minor

Table 4. After Five Cycles, DOX is Adsorbed and Then Desorbed from the Ag-MOF Adsorbent Surface

adsorption/desorption cycle	q_e (adsorption) (mmol/g)	q_e (desorption) (mmol/g)	des. (%)
cycle 1	1.32	1.3	97.16
cycle 2	1.3	1.24	94.1
cycle 3	1.24	1.18	93.9
cycle 4	1.18	1.1	92.04
cycle 5	1.1	0.9	86.17

reduction in regeneration efficacy can be attributed to blocked Ag-MOF sites for adsorption (Figure 12). The chemical stability of the adsorbent was checked by applying PXRD before and after regeneration. The resultant peak did not change, indicating that the stable crystalline nature of the adsorbent. The regeneration effectiveness was determined by eq 6

regeneration effectiveness (%)

$$= \frac{\text{amount of desorbed DOX into the elution solution}}{\text{amount of adsorbed DOX (mmol)}} \times 100 \quad (6)$$

3.2.11. Ag-MOF Adsorbent Testing Using a Sample of Wastewater That Was Not Treated. In Egypt's Port Said industrial district, a sample of raw sewage was obtained from the effluent of a local dyeing plant. Table 5 shows the results of

Table 5. Process of Removing Color from Actual Wastewater Samples Using an Ag-MOF Adsorbent

parameter	unit	before adsorption	after adsorption	% removal
pH		6.7	6.9	
conductivity	$\mu\text{s cm}^{-1}$	882	836	5.21
color	NTU	996	18	98.2
COD		348	22	93.56

the sample's chemical analysis. The experiment was carried out under ideal conditions with no specimen pretreatment. The COD and color were evaluated both before and after the adsorption procedure. The averages from each of the adsorption experiments were kept after being repeated three times.⁵⁵ The viability of Ag-MOF was tested by removing the color from a genuine sample of textile dyeing wastewater to demonstrate its feasibility in a practical setting. Ag-MOF has an excellent color capture capacity, as demonstrated in Table 5 ($\approx 98.2\%$ of color elimination). In addition, the COD concentration decreased from 340 to 19 mg/L. Last but not least, these results are optimistic because the evaluated adsorbent's satisfactory performance (percentage of color removed) confirms our predictions for its effectiveness in applications for wastewater treatment.

3.2.12. Influence of Ionic Strength. The influence of ionic strength on Ag-MOF efficiency against DOX was systematically projected to examination of Ag-MOF efficiency wastewater treatment. The quality of DOX is meaningfully influenced by the amount of other competing ions present in the aqueous solution (Figure S8) (Supporting Information). With a slight decrease in Ag-MOF loading capacity, the

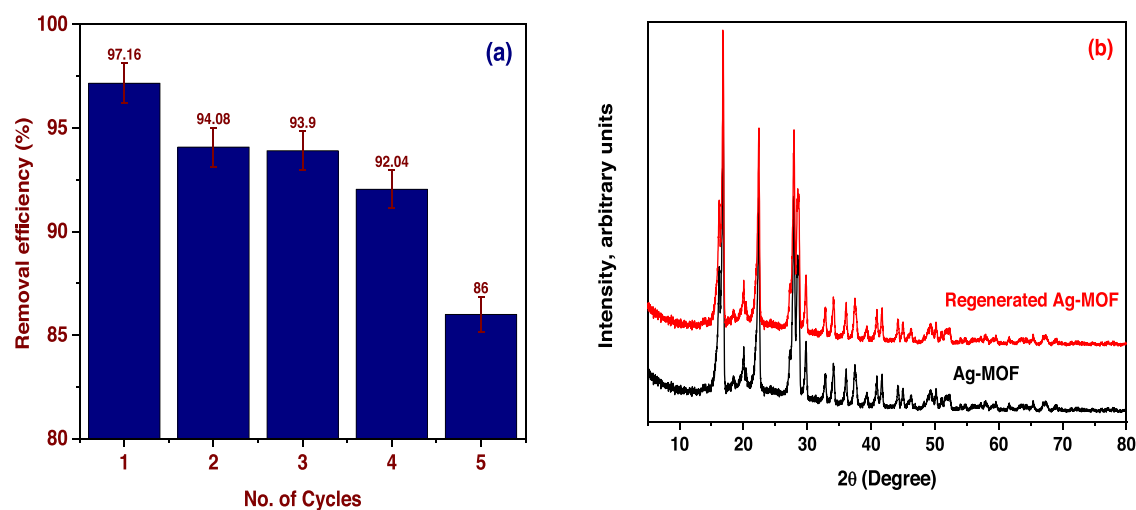


Figure 12. (a) PXRD of Ag-MOF before and after regeneration and (b) reusability efficiency of Ag-MOF.

participant's density has increased (i.e., Cl^-). Adsorption abilities of the adsorbent for DOX are still outstanding at 1.8 mmol/g ($R\% = 85.9\%$). Viewing things broadly, the little discrepancy can be understood as following. DOX molecules engage on the Ag-MOF adsorbent surface as a result of the escalating conflict among negatively charged anionic ions (Cl^-) and negatively charged anions (DOX). In addition, protecting the Ag-MOF surface and reducing the adsorption process were attained by increasing the electrolyte counterion absorption.⁵⁶ Furthermore, the double electric layer contracted as the salinity of the solution increased, generating a repulsive force between the DOX and the adsorbent surface.

3.2.13. Evaluation in Relation to Other Adsorbents. Table S4 (Supporting Information) uses Ag-MOF as the adsorbent for the comparison of its superior DOX adsorption capacity with the remaining adsorbents.⁵⁷ This suggests that DOX has a sizable capacity for Ag-MOF adsorption.

3.3. Biological Activity. **3.3.1. Cytotoxicity Activity.** By using the MTT technique, the cytotoxicity of the investigated Ag-MOF and DOX@Ag-MOF toward human breast cancer cells (MCF-7) was evaluated in vitro. Using various sample concentrations (7.8, 15.6, 31.25, 62.5, 125, 250, and 500 $\mu\text{g}/\text{mL}$) and cell viability (%), the inhibitory efficacy against breast cancer cells (MCF-7) was discovered. The IC_{50} of the investigated substances was determined at 540 nm utilizing a reader for microplates (Table 6).^{57,58} The IC_{50} was found to be 216.8 and 58.6 $\mu\text{g}/\text{mL}$ for Ag-MOF and DOX@Ag-MOF, respectively (Figure 13).^{58,59}

Table 6. Cytotoxicity of Ag-MOF DOX@Ag-MOF against Human Breast Cancer (MCF-7) Cell Lines

conc. $\mu\text{g}/\text{mL}$	cell viability (%)	
	Ag-MOF	DOX@Ag-MOF
7.8	100	100
15.6	99.8	99.6
31.25	98.23	90.2
62.5	88.6	75.9
125	71.7	52.6
250	52.2	33.1
500	39.7	12.2

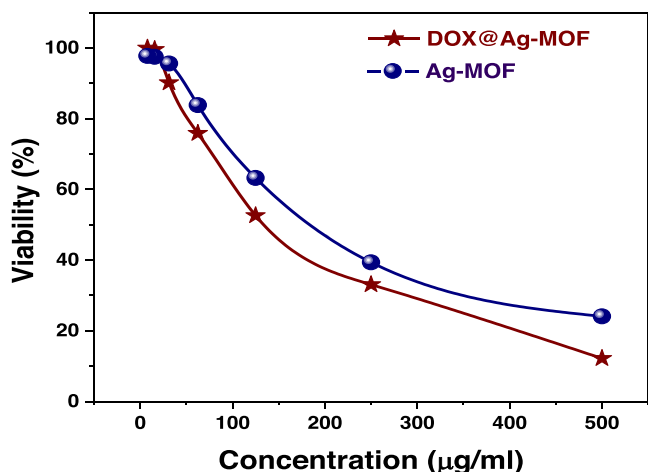


Figure 13. Proportional viability of tumor cells at different Ag-MOF and DOX@Ag-MOF concentrations.

3.3.2. In Vitro Antimicrobial Activity. The ethanol extracts from Ag-MOF and DOX@Ag-MOF are tested using a well-diffused approach for their antifungal and antibacterial effects toward ethanol extracts from *Candida albicans*, *Staphylococcus aureus*, and *Escherichia coli*. The compounds show strong effects, especially DOX@Ag-MOF (Table S5 and Figure 14).^{60,61}

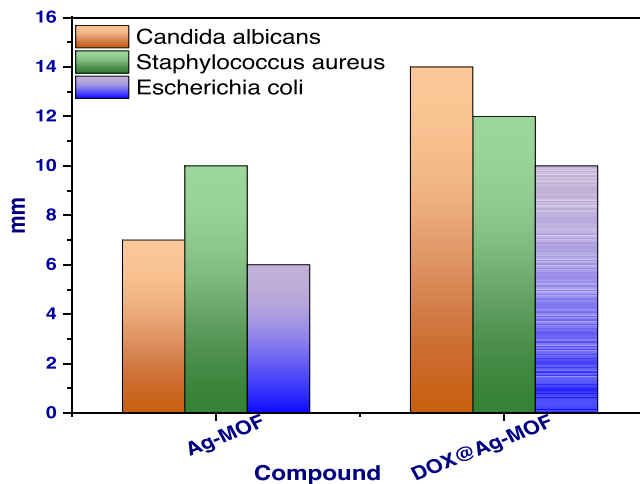


Figure 14. Correlation of the antimicrobial activity results of Ag-MOF and DOX@Ag-MOF toward *C. albicans*, *E. coli*, and *S. aureus*.

4. CONCLUSIONS

The effective synthesis of silver metal–organic frameworks (Ag-MOF) permits for the development of a straightforward but highly effective adsorbent for pharmacological antitumor doxorubicin (DOX) from aqueous solution. XRD, SEM, XPS, BET surface area, and pH_{PZC} were used to characterize the adsorbent. Ag-MOF has a high surface area of 676.059 m^2/g as shown by the BET test results. Experimentally, the adsorptive removal of DOX by Ag-MOF as a model example was investigated using a variety of operating settings. At $\text{pH} = 6$, the results revealed that Ag-MOF had a high clearance of 1.33 to 1.85 mmol/g according to the temperature of the adsorption process from 25 to 45 $^{\circ}\text{C}$. The DOX process for adsorption over Ag-MOF was fitted using the PSORE model, and it was comparable to Langmuir hypothesis. The activation energy of the adsorption, 15.23 kJ/mol, indicates that it is subject to the chemisorption mechanism. The reaction was confirmed to be endothermic and spontaneous by a study of the temperature's effect. The following mechanisms of sorption could be at play: (i) electrostatic forces, (ii) hydrogen bonds, and (iii) n -stacking affinity. Because of charge screening and chloride ion competition, the addition of NaCl has a negligible impact on the adsorption capacities (up to 50 g/L). Additionally, after six consecutive adsorption/desorption periods, Ag-MOF's intended desorption effectiveness was >91.6%. The study's findings provide new information on the prospective application of Ag-MOF for the highly effective removal of an anticancer medicine (DOX) from wastewater.

ASSOCIATED CONTENT

Data Availability Statement

The text contains all necessary information, which is also available on request from the corresponding author.

Supporting Information

The Supporting Information is available free of charge at <https://pubs.acs.org/doi/10.1021/acsomega.3c03523>.

Materials and methods; list of abbreviation; Ag-MOF crystallographic data and binding energy of the component resulted from XPS; DOX adsorption capacities; antibacterial and antifungal action; PXRD pattern; N₂ sorption isotherm; XPS spectra; influence of pH; uptake kinetics; temperature effects; van't Hoff plots; and influence of ionic strength (PDF)

AUTHOR INFORMATION

Corresponding Author

Nashwa M. El-Metwaly – Department of Chemistry, Faculty of Applied Sciences, Umm Al-Qura University, Makkah 21955, Saudi Arabia; Department of Chemistry, Faculty of Science, Mansoura University, Mansoura 35516, Egypt;
orcid.org/0000-0002-0619-6206;
Email: n_elmetwaly00@yahoo.com, nmmohamed@uqu.edu.sa

Authors

Kholood M. Alkhamis – Department of Chemistry, College of Science, University of Tabuk, Tabuk 71474, Saudi Arabia
Meshari M. Aljohani – Department of Chemistry, College of Science, University of Tabuk, Tabuk 71474, Saudi Arabia
Saham F. Ibarhiam – Department of Chemistry, College of Science, University of Tabuk, Tabuk 71474, Saudi Arabia
Yasmeen A. S. Hameed – Department of Chemistry, Faculty of Science, Northern Border University, Arar 73222, Saudi Arabia
Hana M. Abumelha – Department of Chemistry, College of Science, Princess Nourah bint Abdulrahman University, Riyadh 11671, Saudi Arabia
Turki M. Habeebullah – Department of Environment and Health Research, The Custodian of Two Holy Mosques Institute for Hajj and Umrah Research, Umm Al-Qura University, Makkah 21955, Saudi Arabia

Complete contact information is available at:
<https://pubs.acs.org/10.1021/acsomega.3c03523>

Notes

The authors declare no competing financial interest.

ACKNOWLEDGMENTS

Princess Nourah bint Abdulrahman University Researchers Supporting Project number (PNURSP2023R22), Princess Nourah bint Abdulrahman University, Riyadh, Saudi Arabia.

REFERENCES

- (1) Amorim, R.; Vilaça, N.; Martinho, O.; Reis, R. M.; Sardo, M.; Rocha, J.; Fonseca, A. M.; Baltazar, F.; Neves, I. C. Zeolite structures loading with an anticancer compound as drug delivery systems. *J. Phys. Chem. C* **2012**, *116*, 25642–25650.
- (2) Cao, S.-W.; Zhu, Y.-J. Surfactant-free preparation and drug release property of magnetic hollow core/shell hierarchical nanostructures. *J. Phys. Chem. C* **2008**, *112*, 12149–12156.
- (3) El-Desouky, M. G.; El-Bindary, M. A.; El-Bindary, A. A. Effective adsorptive removal of anionic dyes from aqueous solution. *Vietnam J. Chem.* **2021**, *59*, 341–361.
- (4) Bahadur, A.; Saeed, A.; Iqbal, S.; Shoaib, M.; ur Rahman, M. S.; Bashir, M. I.; Asghar, M.; Ali, M. A.; Mahmood, T. Biocompatible waterborne polyurethane-urea elastomer as intelligent anticancer drug

release matrix: a sustained drug release study. *React. Funct. Polym.* **2017**, *119*, 57–63.

(5) Tacar, O.; Sriamornsak, P.; Dass, C. R. Doxorubicin: an update on anticancer molecular action, toxicity and novel drug delivery systems. *J. Pharm. Pharmacol.* **2012**, *65*, 157–170.

(6) He, Q.; Liu, J.; Liang, J.; Liu, X.; Tuo, D.; Li, W. Chemically surface tunable solubility parameter for controllable drug delivery—an example and perspective from hollow PAA-coated magnetite nanoparticles with R6G model drug. *Materials* **2018**, *11*, No. 247.

(7) Shoaib, M.; Bahadur, A.; Saeed, A.; ur Rahman, M. S.; Naseer, M. M. Biocompatible, pH-responsive, and biodegradable polyurethanes as smart anti-cancer drug delivery carriers. *React. Funct. Polym.* **2018**, *127*, 153–160.

(8) Chen, X.; Tong, R.; Shi, Z.; Yang, B.; Liu, H.; Ding, S.; Wang, X.; Lei, Q.; Wu, J.; Fang, W. MOF nanoparticles with encapsulated autophagy inhibitor in controlled drug delivery system for antitumor. *ACS Appl. Mater. Interfaces* **2018**, *10*, 2328–2337.

(9) Balarak, D.; Mahvi, A. H.; Shahbaksh, S.; Wahab, M. A.; Abdala, A. Adsorptive removal of azithromycin antibiotic from aqueous solution by azolla filiculoides-based activated porous carbon. *Nanomaterials* **2021**, *11*, No. 3281.

(10) Vallet-Regi, M.; Colilla, M.; Izquierdo-Barba, I.; Manzano, M. Mesoporous silica nanoparticles for drug delivery: Current insights. *Molecules* **2017**, *23*, No. 47.

(11) Al-Musawi, T. J.; Mahvi, A. H.; Khatibi, A. D.; Balarak, D. Effective adsorption of ciprofloxacin antibiotic using powdered activated carbon magnetized by iron (III) oxide magnetic nanoparticles. *J. Porous Mater.* **2021**, *28*, 835–852.

(12) Li, H.; Zhang, Y.; Liang, L.; Song, J.; Wei, Z.; Yang, S.; Ma, Y.; Chen, W. R.; Lu, C.; Wen, L. Doxorubicin-loaded metal-organic framework nanoparticles as acid-activatable hydroxyl radical nanogenerators for enhanced chemo/chemodynamic synergistic therapy. *Materials* **2022**, *15*, No. 1096.

(13) Ghoochian, M.; Panahi, H. A.; Sobhanardakani, S.; Taghavi, L.; Hassani, A. H. Synthesis and application of Fe₃O₄/SiO₂/thermosensitive/PAMAM-CS nanoparticles as a novel adsorbent for removal of tamoxifen from water samples. *Microchem. J.* **2019**, *145*, 1231–1240.

(14) Guan, X.; Li, Y.; Jiao, Z.; Chen, J.; Guo, Z.; Tian, H.; Chen, X. A pH-sensitive charge-conversion system for doxorubicin delivery. *Acta Biomater.* **2013**, *9*, 7672–7678.

(15) Althumayri, K.; Guesmi, A.; El-Fattah, W. A.; Khezami, L.; Soltani, T.; Hamadi, N. B.; Shahat, A. Effective adsorption and removal of doxorubicin from aqueous solutions using mesostructured silica nanospheres: Box-Behnken design optimization and adsorption performance evaluation. *ACS Omega* **2023**, *8*, 14144–14159.

(16) Kiwaan, H. A.; Mohamed, F. S.; El-Ghamaz, N. A.; Beshry, N. M.; El-Bindary, A. A. Experimental and electrical studies of Na-X zeolite for the adsorption of different dyes. *J. Mol. Liq.* **2021**, *332*, No. 115877.

(17) Zhou, Y.; Quan, G.; Wu, Q.; Zhang, X.; Niu, B.; Wu, B.; Huang, Y.; Pan, X.; Wu, C. Mesoporous silica nanoparticles for drug and gene delivery. *Acta Pharm. Sin. B* **2018**, *8*, 165–177.

(18) Nguyen, T. N.; Nguyen, T. T.; Nghiem, T. H. L.; Nguyen, D. T.; Tran, T. T. H.; Vu, D.; Nguyen, T. B. N.; Nguyen, T. M. H.; Nguyen, V. T.; Nguyen, M. H. Optical properties of doxorubicin hydrochloride load and release on silica nanoparticle platform. *Molecules* **2021**, *26*, No. 3968.

(19) El-Metwaly, N. M.; Katouah, H. A.; El-Desouky, M. G.; El-Bindary, A. A.; El-Bindary, M. A. Fabricating of Fe₃O₄@Ag-MOF nanocomposite and evaluating its adsorption activity for removal of doxorubicin. *J. Environ. Sci. Health, Part A* **2022**, *57*, 1099–1115.

(20) Aljohani, M. M.; Al-Qahtani, S. D.; Alshareef, M.; El-Desouky, M. G.; El-Bindary, A. A.; El-Metwaly, N. M.; El-Bindary, M. A. Highly efficient adsorption and removal bio-staining dye from industrial wastewater onto mesoporous Ag-MOFs. *Process Saf. Environ. Prot.* **2023**, *172*, 395–407.

(21) Mogharbel, R. T.; Alkhamis, K.; Felaly, R.; El-Desouky, M. G.; El-Bindary, A. A.; El-Metwaly, N. M.; El-Bindary, M. A. Superior

- adsorption and removal of industrial dye from aqueous solution via magnetic silver metal-organic framework nanocomposite. *Environ. Technol.* **2023**, 1–17.
- (22) Alsuhaibani, A. M.; Refat, M. S.; Adam, A. M. A.; El-Desouky, M. G.; El-Bindary, A. A. Enhanced adsorption of ceftriaxone antibiotics from water by mesoporous copper oxide nanosphere. *Desalin. Water Treat.* **2023**, 281, 234–248.
- (23) Alsharief, H. H.; Alatawi, N. M.; Al-bonayan, A. M.; Alrefae, S. H.; Saad, F. A.; El-Desouky, M. G.; El-Bindary, A. A. Adsorption of Azorubine E122 dye via Na-mordenite with tryptophan composite: batch adsorption, Box-Behnken design optimisation and antibacterial activity. *Environ. Technol.* **2023**, 1–20.
- (24) Al-Hazmi, G. H.; Adam, A. M. A.; El-Desouky, M. G.; El-Bindary, A. A.; Alsuhaibani, A. M.; Refat, M. S. Efficient Adsorption of Rhodamine B using a composite of Fe₃O₄@ZIF-8: Synthesis, characterization, modelling analysis, statistical physics and mechanism of interaction. *Bull. Chem. Soc. Ethiop.* **2023**, 37, 211–229.
- (25) Al-Hazmi, G. A. A.; El-Zahhar, A. A.; El-Desouky, M. G.; El-Bindary, M. A.; El-Bindary, A. A. Adsorption of industrial dye onto a zirconium metal-organic framework: synthesis, characterization, kinetics, thermodynamics, and DFT calculations. *J. Coord. Chem.* **2022**, 75, 1203–1229.
- (26) Alrefae, S. H.; Aljohani, M.; Alkhamis, K.; Shaaban, F.; El-Desouky, M. G.; El-Bindary, A. A.; El-Bindary, M. A. Adsorption and effective removal of organophosphorus pesticides from aqueous solution via novel metal-organic framework: Adsorption isotherms, kinetics, and optimization via Box-Behnken design. *J. Mol. Liq.* **2023**, 384, No. 122206.
- (27) El-Desouky, M. G.; Shahat, A.; El-Bindary, A. A.; El-Bindary, M. A. Description, kinetic and equilibrium studies of the adsorption of carbon dioxide in mesoporous iron oxide nanospheres. *Biointerface Res. Appl. Chem.* **2022**, 12, 1022–1038.
- (28) El-Desouky, M. G.; Khalil, M. A. G.; El-Afify, M. A. M.; El-Bindary, A. A.; El-Bindary, M. A. Effective methods for removing different types of dyes - modelling analysis statistical physics treatment and DFT calculations: a review. *Desalin. Water Treat.* **2022**, 280, 89–127.
- (29) El-Bindary, M. A.; El-Desouky, M. G.; El-Bindary, A. A. Metal-organic frameworks encapsulated with an anticancer compound as drug delivery system: Synthesis, characterization, antioxidant, anticancer, antibacterial, and molecular docking investigation. *Appl. Organomet. Chem.* **2022**, 36, No. e6660.
- (30) El-Bindary, M. A.; El-Desouky, M. G.; El-Bindary, A. A. Adsorption of industrial dye from aqueous solutions onto thermally treated green adsorbent: A complete batch system evaluation. *J. Mol. Liq.* **2022**, 346, No. 117082.
- (31) El-Bindary, A. A.; El-Desouky, M. G.; El-Afify, M. A. M. Thermal and spectroscopic studies of some prepared metal complexes and investigation of their potential anticancer and antiviral drug activity against SARS-CoV-2 by molecular docking simulation. *Biointerface Res. Appl. Chem.* **2022**, 12, 1053–1075.
- (32) Al-Wasidi, A. S.; AlZahrani, I. I. S.; Thawibaraka, H. I.; Naglah, A. M.; El-Desouky, M. G.; El-Bindary, M. A. Adsorption studies of carbon dioxide and anionic dye on green adsorbent. *J. Mol. Struct.* **2022**, 1250, No. 131736.
- (33) Oladoye, P. O.; Adegboyega, S. A.; Giwa, A.-R. A. Remediation potentials of composite metal-organic frameworks (MOFs) for dyes as water contaminants: A comprehensive review of recent literatures. *Environ. Nanotechnol., Monit. Manage.* **2021**, 16, No. 100568.
- (34) Adegoke, K. A.; Akinawo, S. O.; Adebuseyi, T. A.; Ajala, O. A.; Adegoke, R. O.; Maxakato, N. W.; Bello, O. S. Modified biomass adsorbents for removal of organic pollutants: a review of batch and optimization studies. *Int. J. Environ. Sci. Technol.* **2023**, 1–30.
- (35) Al-Hazmi, G. H.; Refat, M. S.; El-Desouky, M. G.; El-Bindary, A. A. Effective adsorption and removal of industrial dye from aqueous solution using mesoporous zinc oxide nanoparticles via metal organic framework: equilibrium, kinetics and thermodynamic studies. *Desalin. Water Treat.* **2022**, 272, 277–289.
- (36) Langmuir, I. The constitution and fundamental properties of solids and liquids. Part I. Solids. *J. Am. Chem. Soc.* **1916**, 38, 2221–2295.
- (37) Freundlich, H. M. F. Over the adsorption in solution. *J. Phys. Chem. A* **1906**, 57, 385–471.
- (38) Dubinin, M. The equation of the characteristic curve of activated charcoal. *Proc. Acad. Sci. USSR Phys. Chem. Sect.* **1947**, 55, 327–329.
- (39) Redlich, O.; Peterson, D. L. A useful adsorption isotherm. *J. Phys. Chem. A* **1959**, 63, 1024.
- (40) Tempkin, V. P. M. I. Kinetics of ammonia synthesis on promoted iron catalyst. *Acta Phys. Chim. USSR* **1940**, 12, 327–356.
- (41) Al-Hazmi, G. H.; El-Desouky, M. G.; El-Bindary, A. A. Synthesis, Characterization and Microstructural Evaluation of ZnO nanoparticles by William-Hall and size-strain plot methods. *Bull. Chem. Soc. Ethiop.* **2022**, 36, 815–829.
- (42) Lagergren, S. K. About the theory of so-called adsorption of soluble substances. *Sven. Vetenskapskad. Handlingar* **1898**, 24, 1–39.
- (43) Ho, Y.-S.; McKay, G. Pseudo-second order model for sorption processes. *Process Biochem.* **1999**, 34, 451–465.
- (44) Weber, W. J., Jr; Morris, J. C. Kinetics of adsorption on carbon from solution. *J. Sanit. Eng. Div.* **1963**, 89, 31–59.
- (45) Vlad, M.; Segal, E. A kinetic analysis of Langmuir model for adsorption within the framework of Jovanovic theory; a generalization of the Jovanovic isotherm. *J. Surf. Sci.* **1979**, 79, 608–616.
- (46) Al-Hazmi, G. A. A.; El-Zahhar, A. A.; El-Desouky, M. G.; El-Bindary, A. Superior adsorption and removal of doxorubicin from aqueous solution using activated carbon via thermally treated green adsorbent: isothermal, kinetic, and thermodynamic studies. *Environ. Technol.* **2022**, 1–20.
- (47) Al-Hazmi, G. A. A.; El-Bindary, M. A.; El-Desouky, M. G.; El-Bindary, A. A. Efficient adsorptive removal of industrial dye from aqueous solution by synthesized zeolitic imidazolate framework-8 loaded date seed activated carbon and statistical physics modeling. *Desalin. Water Treat.* **2022**, 258, 85–103.
- (48) Al-Hazmi, G. A. A.; AbouMelha, K. S.; El-Desouky, M. G.; El-Bindary, A. A. Effective adsorption of doxorubicin hydrochloride on zirconium metal-organic framework: Equilibrium, kinetic and thermodynamic studies. *J. Mol. Struct.* **2022**, 1258, No. 132679.
- (49) El-Wahab, M. A.; El-Desouky, M. G. Study the effect of antioxidants on biological activity and on homopolypropylene; mechanical and physical properties. *J. Indian Chem. Soc.* **2022**, 99, No. 100764.
- (50) Al-Hazmi, G. A. A.; El-Zahhar, A. A.; El-Desouky, M. G.; El-Bindary, M. A.; El-Bindary, A. A. Efficiency of Fe₃O₄@ZIF-8 for the removal of Doxorubicin from aqueous solutions: equilibrium, kinetics and thermodynamic studies. *Environ. Technol.* **2022**, 1–20.
- (51) El-Desouky, M. G.; Hassan, N.; Shahat, A.; El-Didamony, A.; El-Bindary, A. A. Synthesis and characterization of porous magnetite nanosphere iron oxide as a novel adsorbent of anionic dyes removal from aqueous solution. *Biointerface Res. Appl. Chem.* **2021**, 11, 13377–13401.
- (52) El-Desouky, M. G.; El-Bindary, A. A. Magnetic metal-organic framework (Fe₃O₄@ZIF-8) nanocomposites for adsorption of anionic dyes from wastewater. *Inorg. Nano-Met. Chem.* **2021**, 1–15.
- (53) Al-Wasidi, A. S.; AlZahrani, I. I. S.; Naglah, A. M.; El-Desouky, M. G.; Khalil, M. A.; El-Bindary, A. A.; El-Bindary, M. A. Effective Removal of Methylene Blue From Aqueous Solution Using Metal-Organic Framework; Modelling Analysis, Statistical Physics Treatment and DFT Calculations. *ChemistrySelect* **2021**, 6, 11431–11447.
- (54) Hassan, N.; Shahat, A.; El-Didamony, A.; El-Desouky, M. G.; El-Bindary, A. A. Equilibrium, Kinetic and Thermodynamic studies of adsorption of cationic dyes from aqueous solution using ZIF-8. *Moroccan J. Chem.* **2020**, 8, 624–635.
- (55) Hassan, N.; Shahat, A.; El-Didamony, A.; El-Desouky, M. G.; El-Bindary, A. A. Synthesis and characterization of ZnO nanoparticles via zeolitic imidazolate framework-8 and its application for removal of dyes. *J. Mol. Struct.* **2020**, 1210, No. 128029.

(56) Hassan, N.; Shahat, A.; El-Didamony, A.; El-Desouky, M. G.; El-Bindary, A. A. Mesoporous iron oxide nano spheres for capturing organic dyes from water sources. *J. Mol. Struct.* **2020**, *1217*, No. 128361.

(57) Kasula, M.; Le, T.; Thomsen, A.; Esfahani, M. R. Silver metal organic frameworks and copper metal organic frameworks immobilized on graphene oxide for enhanced adsorption in water treatment. *Chem. Eng. J.* **2022**, *439*, No. 135542.

(58) El-Desouky, M. G.; El-Bindary, A. A.; El-Afify, M. A. M.; Hassan, N. Synthesis, characterization, theoretical calculation, DNA binding, molecular docking, anticovid-19 and anticancer chelation studies of some transition metal complexes. *Inorg. Nano-Met. Chem.* **2022**, *52*, 1273–1288.

(59) El-Desouky, M. G.; Khalil, M. A.; El-Bindary, A. A.; El-Bindary, M. A. Biological, biochemical and thermochemical techniques for biofuel production: An updated review. *Biointerface Res. Appl. Chem.* **2022**, *12*, 3034–3054.

(60) Livesey, T. C.; Mahmoud, L. A. M.; Katsikogianni, M. G.; Nayak, S. Metal-Organic frameworks and their biodegradable composites for controlled delivery of antimicrobial drugs. *Pharmaceutics* **2023**, *15*, No. 274.

(61) Vodyashkin, A. A.; Sergorodceva, A. V.; Kezimana, P.; Stanishevskiy, Y. M. Metal-Organic Framework (MOF)—A Universal Material for Biomedicine. *Int. J. Mol. Sci.* **2023**, *24*, No. 7819.